Available online at www.sciencedirect.com
ScienceDirect
Physics of the Earth and Planetary Interiors 164 (2007) 21–35
PHYSICS OF THE EARTH AND PLANETARY INTERIORS
www.elsevier.com/locate/pepi

Source field effects in the auroral zone: Evidence from the Slave craton (NW Canada)

Pamela Lezaeta [a,*], Alan Chave [a,1], Alan G. Jones [b,3], Rob Evans [a,2]

[a] *Woods Hole Oceanographic Institution, Woods Hole, MA 02543, USA*
[b] *Geological Survey of Canada, 615 Booth Street, Ottawa, Ont., Canada K1A0E9*

Received 18 September 2006; received in revised form 24 April 2007; accepted 11 May 2007

Abstract

We present an investigation of source field effects on the magnetic fields from multiple long period magnetotelluric (MT) data collected on the floors of lakes throughout the Slave craton (NW Canada) from 1998 to 2000. Monthly and daily power spectra of the magnetic fields suggest a dynamic and seasonally varying source, with atypical geomagnetic activity in year 2000. Bounded influence MT and GDS responses were obtained for periods ranging between 80 and 25,000 s over selected monthly time segments. The responses at periods over 4000 s vary, suggesting source field effects.

A frequency domain principal component (PC) method was applied to the array to investigate the spatial form of the source field variations. The PC analysis was tested with synthetic data from a regional 3D model with a uniform external source to study the sensitivity of the eigenvectors to conductivity structure, demonstrating a negligible influence with increasing penetration depth. We conclude that magnetic fields at periods near one half day are subject to a 1D polarized source of relatively homogeneous morphology over the survey area during any month recorded, except for the summer month of July 2000 that had particularly high geomagnetic activity. In general, the source space approaches two polarizations at periods below one half day, with the dominant NS component seen quasi-homogeneous over the survey area at periods over 1000 s.

Keywords: Geomagnetic deep sounding (GDS); Magnetotelluric (MT); Geomagnetic field perturbation; Principal components

1. Introduction

The time variations of the electric and magnetic fields measured at Earth's surface are dependent both on sub-surface electrical conductivity variations and upon the spatial morphology and temporal variability of the source field incident at the Earth–air interface. If the source is a plane wave (i.e., of infinite transverse wavelength), then electromagnetic induction in the conductive Earth is independent of the source morphology (wavelength independent). Determination of the electrical conductivity of Earth's crust and mantle is the target in the application of the magnetotelluric (MT)

* Corresponding author now at: Earth Sciences, Boston University, 675 Commonwealth Ave., Boston, MA 02215, USA.
E-mail addresses: plezaeta@whoi.edu, plezaeta@cox.net (P. Lezaeta).
[1] Address: MS#7, Department of Applied Ocean Physics and Engineering, Woods Hole Oceanographic Institution, Woods Hole, MA 02543, USA.
[2] Address: MS#24, Geology & Geophysics Department, Woods Hole Oceanographic Institution, USA.
[3] Address: School of Cosmic Physics, Dublin Institute for Advanced Studies, 5 Merrion Square, Dublin 2, Ireland.

0031-9201/$ – see front matter © 2007 Elsevier B.V. All rights reserved.
doi:10.1016/j.pepi.2007.05.002

and geomagnetic depth sounding (GDS) methods. It is well known that under several conditions (e.g., when the distance to the source currents is much larger than the depth of interest and when the horizontal wavelength of the source is much larger than the horizontal scale of the study region), the source can be considered as quasi-homogeneous, and hence can be approximated as a plane wave (e.g., Vozoff, 1972). Dmitriev and Berdichevsky (1979) showed for 1D conductivity Earth models that not only is induction independent of the source morphology for plane waves (i.e., of zero wavenumber), but also for linearly varying and odd-order wavenumber sources when their wavelengths are comparatively long. The assumption of uniform sources becomes most valid at mid-latitude sites distant from the equatorial and auroral electrojets, although quantification of this statement has been limited. Short wavelength sources are believed to be associated with energetic, transient events during active periods in areas close to the equatorial and auroral electrojets (e.g., Mareschal, 1986). This can lead to considerable difficulty in estimating the MT or GDS responses even using modern processing methods (Garcia et al., 1997).

Experience has shown that MT observations recorded over a long period of time (to allow many tens to hundreds of statistical realizations to be combined) have a better chance of compensating non-homogeneous source field effects, resulting in a quasi-homogeneous response (e.g., Engels, 1997). This is generally true at mid-latitudes, whereas at high-latitudes this approach has to be used with caution (e.g., Mareschal, 1986). Near regions of localized ionospheric currents, Viljanen et al. (1993) showed that the average of electromagnetic amplitudes over time cannot remove source field effects on the MT responses but could only reduce them. Near the auroral zone, non-homogeneous sources can be a problem for understanding electromagnetic induction. For example, in Scandinavia, the BEAR Working Group invoked a dynamic (time varying) source to explain array observations (Engels et al., 2002). Garcia et al. (1997) showed for a high latitude zone of Canada that the bounded influence algorithm of Chave and Thomson (2004) could successfully eliminate auroral storm events of short wavelength from the night sector while still leaving the more homogeneous events from the day sector, although in extreme cases this approach broke down. Jones and Spratt (2002) used the vertical component of the magnetic field time series for eliminating highly disturbed intervals of auroral origin, successfully reducing source effects in the MT responses under weak lateral conductivity contrasts (i.e., 1D sub-surface approach). From a 1 year GDS survey performed in Greenland, Engels (1997) concluded that the induction arrows at periods below 2000 s represent the responses of quasi-homogeneous sources. At longer periods, non-homogeneous effects became evident in this data set, but they could be compensated by processing the time series robustly over a year. Engels (1997) further asserted that the induction arrows were more sensitive to Earth conductivity variations (and hence to induction) than to source geometry.

Egbert and Booker (1989) used an array-based empirical orthogonal function or principal component approach to obtain multiple-site transfer functions under the assumption that the external source is low in dimension. In that work, it was demonstrated for a particular mid-latitude array that the largest eigenvalues of the spectral density matrix define the spatial dimension of a plane wave source field (i.e., two large eigenvalues for a uniform source of two polarizations), while the remaining smaller eigenvalues represent non-homogeneous sources and/or cultural and instrumental noise. Egbert (1989) based this conclusion on synthetic data generated for randomly varying electromagnetic sources over a homogeneous 1D Earth and on field data (Egbert and Booker, 1989).

We will consider MT and GDS data from 2-year-long campaigns using seafloor instrumentation deployed in lakes from float airplanes on the Slave craton, which is located in NW Canada in the midst of the auroral zone (Fig. 1). The measurements were obtained with the aim of investigating the three-dimensional (3D) electrical conductivity structure of the Slave mantle (Jones et al., 2003). An extensive suite of geophysical, geochemical/petrologic and geologic studies have been carried out in recent years by Lithoprobe and the Geological Survey of Canada on the Slave with the aim of understanding the nature of its Archean lithosphere, which is the oldest part of North America. In addition, interest in the Slave from the mining industry has increased because of the discovery of diamondiferous kimberlites in the early 1990s.

In this paper, we focus on understanding the behavior of the source fields and their effect on the MT/GDS responses through the analysis of long period array data. Section 2 presents the data and describes monthly power spectra at each site. Section 3 presents selected time series of disturbed and quiet events, showing their correlation with a global magnetic activity index and daily power spectra. Section 4 discusses the magnetotelluric and geomagnetic transfer functions estimated over seasonal intervals and over a full year. Section 5 describes a principal component (PC) method and its application to synthetic data from a regional 3D model for a uniform

source to investigate the sensitivity of the PCs to induction. This is found to be weak for long period data, and hence the PC analysis was applied to the Slave magnetic field data to gain insight into the spatial structure of the source. Section 6 discusses remaining questions.

2. Slave data set

Nineteen stations were recorded in 2-year-long field campaigns at the bottom of selected Slave lakes using shallow water (< 1000 m) ocean bottom instrumentation built at the Woods Hole Oceanographic Institution (Fig. 1). The 2-year arrays span in the Slave craton between latitudes 62–68°N, inside and south of the auroral oval (65–75°N). The instruments were deployed from float airplanes during the summertime when the lakes were ice-free, and recovered a year later. The first survey took place from the summer of 1998–1999 and the second survey was carried out between the summers of 1999 and 2000. Each instrument was programmed to record the two orthogonal horizontal electric fields and the three-component magnetic field at a high sampling rate (∼2 s) during the first month of the survey, switching then automatically to a lower (∼28 s) sampling rate until its retrieval. In this work, we will concentrate on the low sampling rate data. During the first year, data at ten sites were recorded. Nine additional sites were recorded during the second year (Fig. 1). Sites Snare and Point from the first year yielded only three months of reliable time series recorded in the fall. Snare was repeated in the second year, obtaining high quality long period data from October 1999 to July 2000. Thus, point will not be further considered in the following. The time frame for recording good quality data at the low sampling rate varied from site to site due in part to minor instrument problems. In the first year, this ran from October–December of 1998 to June–July of 1999. The time frame for the second year survey was more consistent among sites and of longer duration because the stations were retrieved later in the summer.

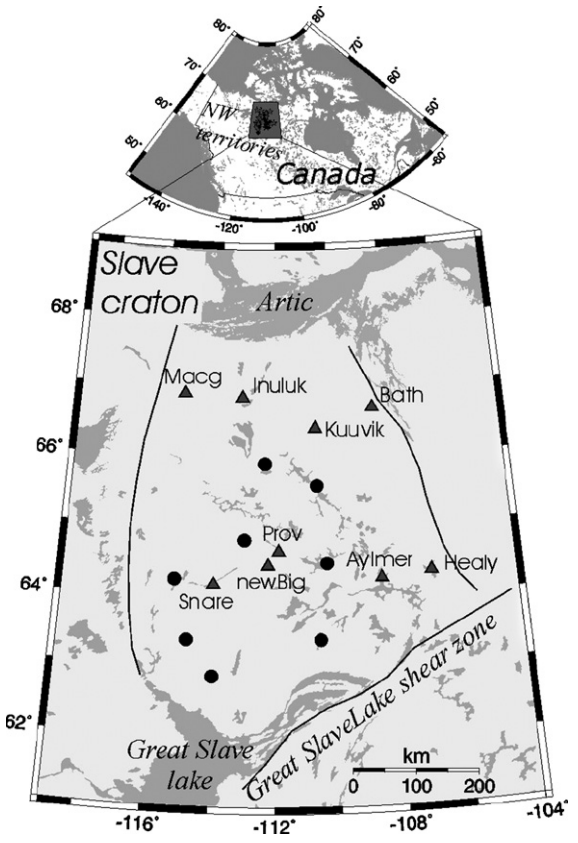

Fig. 1. Location of magnetotelluric stations deployed on the bottom of lakes on the Slave craton. Black dots show the sites from the first year survey (from 1998 to 1999), while triangles refer to the second year survey (1999–2000). Site names are indicated as a reference for Fig. 3. Inset above shows the regional map of Canada.

The magnetic field time series were edited to remove obvious instrumental problems, rotated to correct for instrument tilt, and high pass filtered for drift correction. The cleaned time series were rotated to geomagnetic coordinates and monthly power spectra of the geomagnetic north and east field components at each site were obtained. Figs. 2 and 3 show the east components (B_y) for a period of 3600 s for the first and second years, respectively. The highest power occurred during the summertime (July), especially in the year 2000 which had more solar activity than the previous year, as shown by larger K_p values. Low power is seen for the month of December 1999 (Fig. 2) and March 2000 (Fig. 3), where the K_p index was also very low. The geomagnetic north (B_x) component at 1000–10,000 s periods follows similar trends, but with power spectra 1 or 2 orders of magnitude higher than for B_y (Figs. 2 and 3 for B_y). This is also true for power spectra at longer periods ($> 10,000$ s). In contrast, power spectra at short periods (100–1000 s) from the second year survey have a maximum during the winter time, surpassing by over two orders of magnitude the spectra from spring and summer of 2000 (not shown here). The power spectra for B_x and B_y are comparable at short periods, while the B_x spectra at longer periods surpasses that of B_y by over one order of magnitude. All of this clearly indicates temporal source field variations of different nature depending on the period band under consideration. It has typically been observed that the north component is stronger in auroral zones because of the dominantly east–west form of the low altitude electrojet (Mareschal, 1986). For the Slave data, B_x is the strong component, except at short peri-

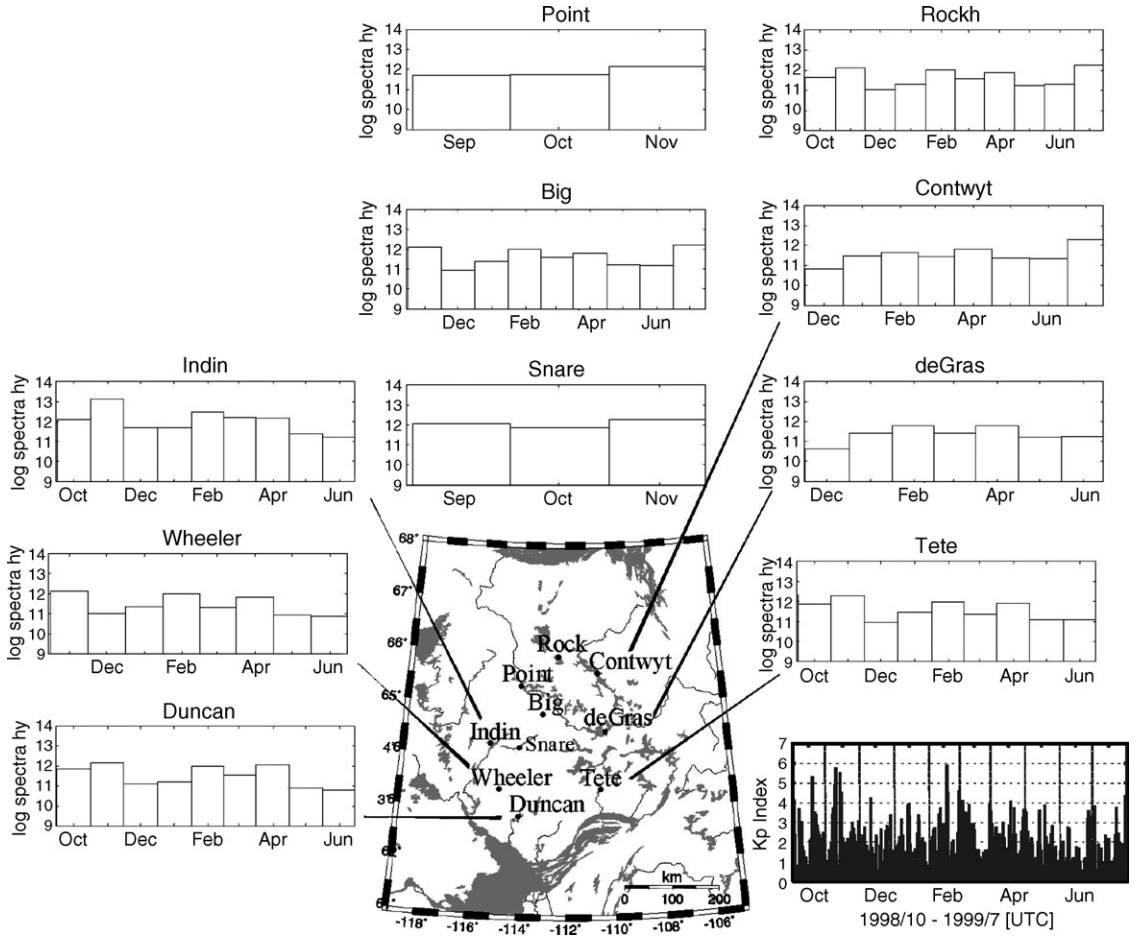

Fig. 2. Log power spectra ($\log(nT^2/H_z)$) for a representative long period (3600 s) for the east geomagnetic field component (B_y) calculated for monthly time segments at selected sites spanning the Slave Province from the first year deployment. The plot at bottom right shows the K_p index of global geomagnetic disturbance (at 3 h sample rate).

ods (below 1000 s), where the source seems governed by a different principle. Monthly power spectra at periods below 1000 s are not well correlated with the global geomagnetic disturbance level (K_p index) as they are for longer periods. This is not a complete surprise as K_p is estimated using a 3 h sampling interval.

3. Time series, power spectra and geomagnetic activity

We have selected a representative site from the second year survey to show time variations of the horizontal and vertical magnetic components over two specific months; March and July 2000. The former represents a quiet time around the equinox and the latter a disturbed time near solstice. As March has no particularly strong geomagnetic activity ($K_p < 4$), the time field variations are more regular (Fig. 4; left). July shows some large disturbances around mid-month ($K_p > 4$; Fig. 4; right), reflecting the Bastille Day geomagnetic storm occurred July 15–16. The time variations for 2000 fluctuate much more drastically over the seasons than during 1999. March for both years was low in solar activity, while the month of July 2000, was the most active.

Such conclusions become more evident from analyzing daily power spectra of the horizontal magnetic field components at 3600 s period. Fig. 5 shows the spectra for a representative site. All highly energetic daily events observed in the magnetic fields occur nearly simultaneously among the sites, indicating a regional disturbance of external origin, as also the daily power spectra are highly correlated with the K_p index (Fig. 5; bottom).

Significant seasonal fluctuations in power are also observed. For example, the peak daily power spectrum from Providence Lake in July 2000 is three orders of magnitude larger than in March 2000 (not shown) at

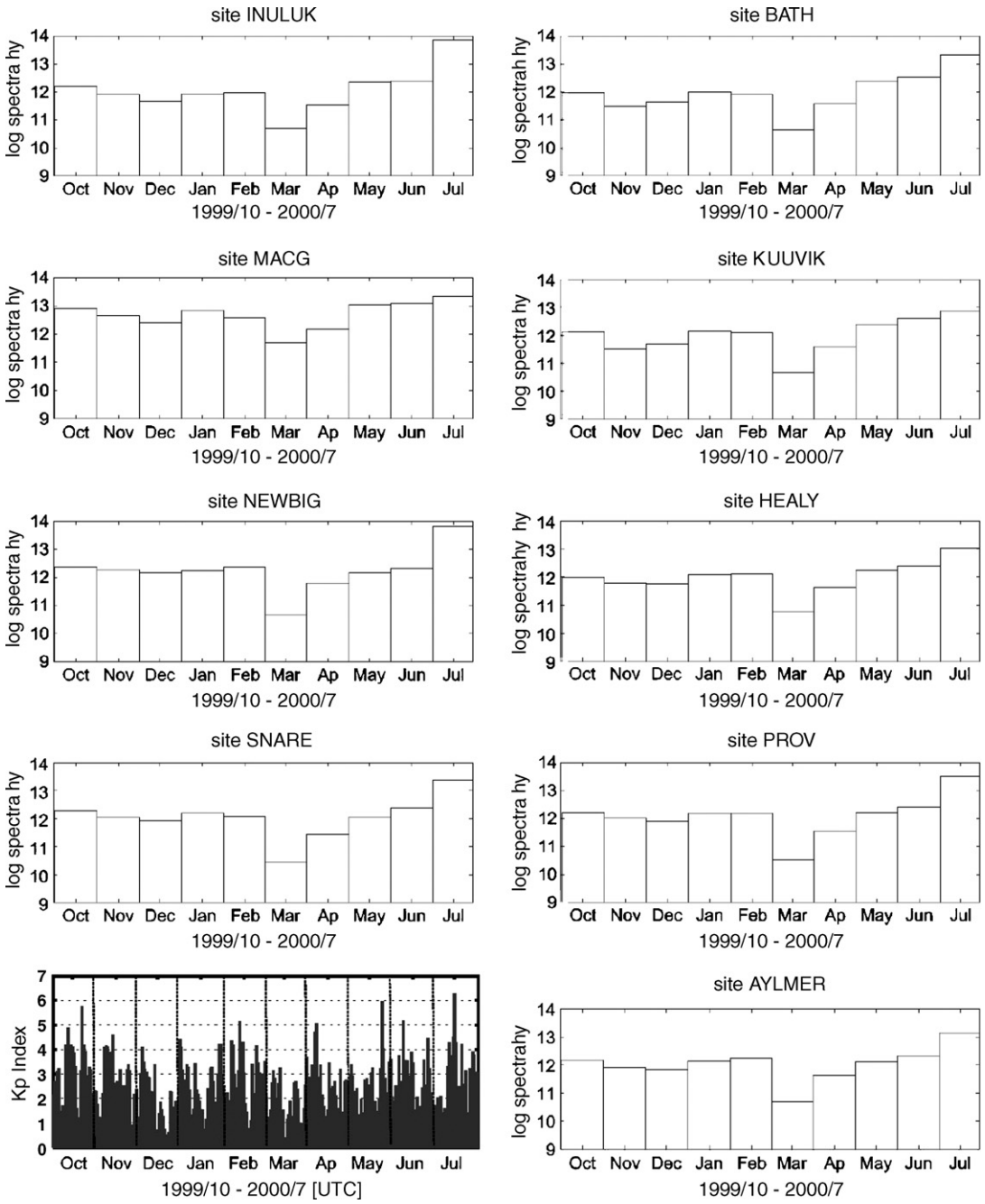

Fig. 3. Power spectra as in Fig. 2 but for sites from the second year survey. The location of the data are shown in Fig. 1.

a period of 3600 s (Fig. 5). At shorter periods, power spectra for March (Fig. 6) are also significantly smaller than those from the month of July at the same period. However, the short period power spectrum for July (not shown) does not correlate with the K_p index. This may hint at another type of external source below 1000 s as compared to longer periods during that summer, while in March it seems that the same external source morphology is affecting all periods, as their trends correlate with the daily K_p variations (Fig. 6 for a short period).

If non-homogeneous sources are influencing electromagnetic induction in the survey area, we should be able to see differences between the frequency domain

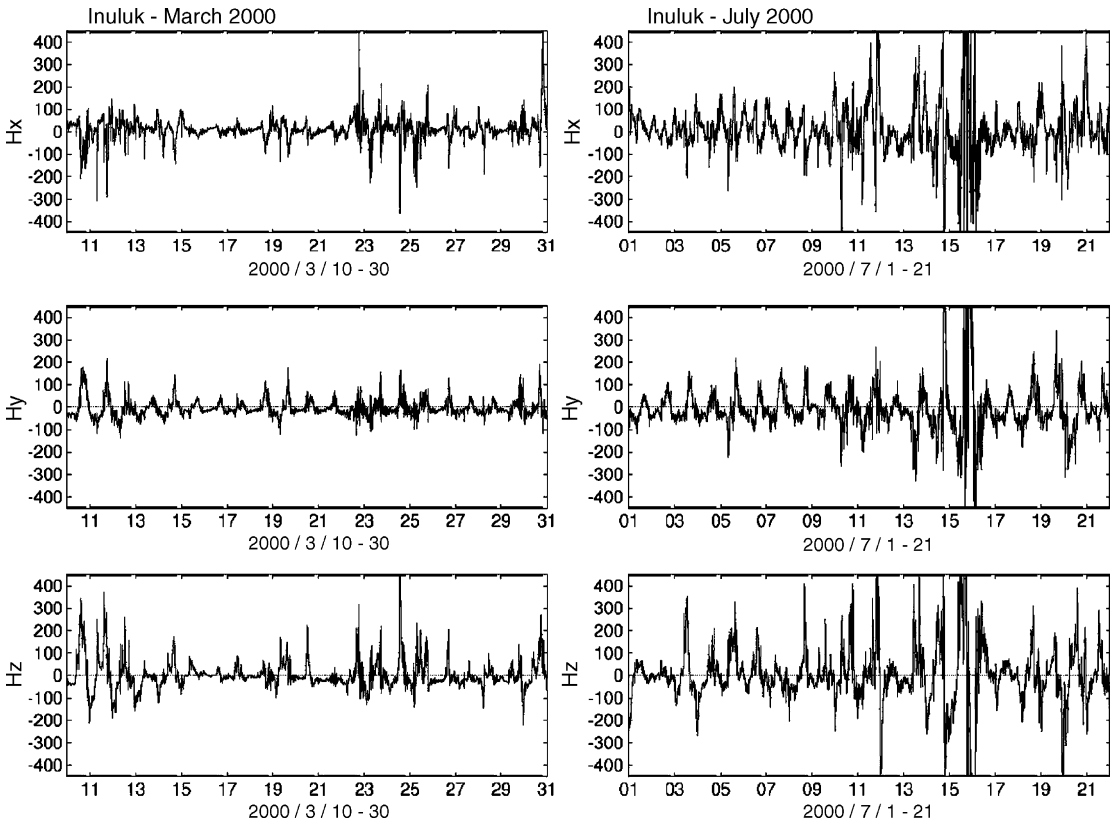

Fig. 4. Time variations of the horizontal and vertical magnetic field components (in nT) during the month of March (left) and July (right) of 2000 measured at Inuluk. The rows from top to bottom are the geomagnetic north, east and vertical components, respectively. The location of Inuluk is shown in Fig. 1.

MT/GDS responses obtained from data segments over different seasons.

4. Transfer functions from seasonal segments

Induction arrows represent the vector sum over the magnetic transfer functions of both horizontal components of either real or imaginary parts. These are sensitive to lateral changes in Earth's electrical conductivity, increasing in length as the conductivity contrast increases at the penetration depths of the current induced by the external source. If the external source is plane wave or uniform, then the induction arrows should point away from zones of higher conductivity using Wiese's convention (Schmucker, 1973). However, any non-homogeneous external source could contribute to deviations of the direction and length of induction arrows, as the induction scale becomes dependent on the wavelength of the source and hence vertical b-field components not associated with Earth's lateral conductivity variations arise.

Fig. 7 shows the induction arrows at a period of 5000 s for all sites of both the first and second years. The transfer functions were obtained by processing the time series using a bounded influence algorithm (Chave and Thomson, 2004) appropriate for eliminating anomalous magnetic field segments. Arrows at different gray tones correspond to estimates from seasonal time series segments of good quality; light gray for spring time, dark for winter and black for all good quality segments over 8–9 months of recording (from October–November to August; Fig. 7). At shorter periods, the different arrows tend to converge to a common direction, thus suggesting that non-homogeneous source effects are weaker. It is remarkable how the long period arrows obtained over all months represent, for most sites, an average of the induction arrows obtained from the seasonal segments. This suggests that the external source is affecting the induction arrows at long periods (over 4000 s). However, processing over several seasons seems to compensate for non-homogeneous source effects that are evident in shorter time segments. Note also that the seasonal induction arrows from the second year survey display far more

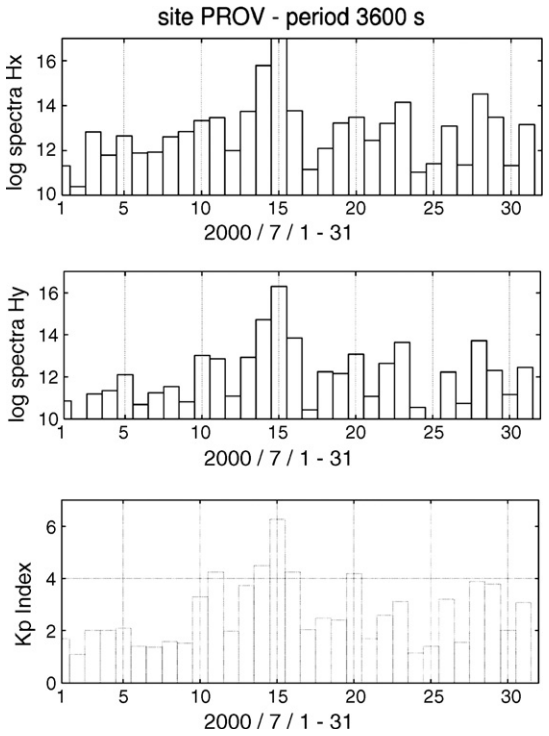

Fig. 5. Daily power spectra ($\log(nT^2/H_z)$) at a period of 3600 s for the horizontal magnetic field components during the month of July 2000 measured at Prov. The first two rows from top to bottom are the geomagnetic north and east components, respectively. The bottom row shows the K_p index at a 1 day sample rate over the month.

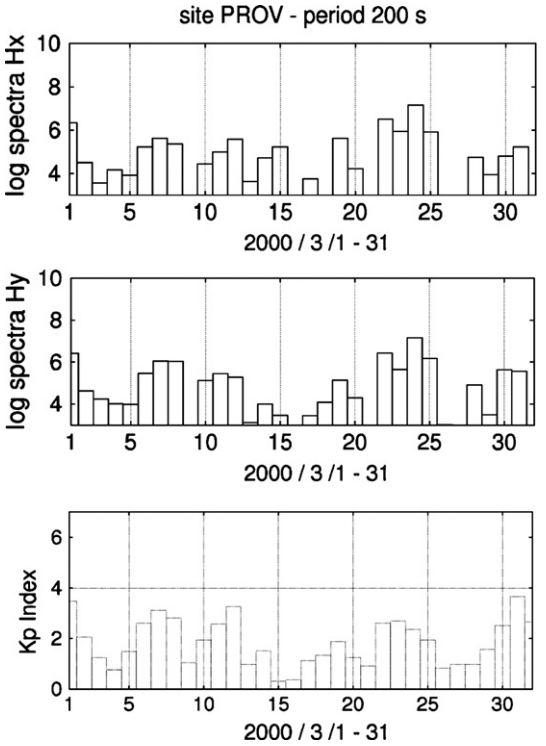

Fig. 6. As for Fig. 5 but for daily power spectra (log scale) at a period of 200 s during the month of March 2000. The bottom row shows the K_p index over the month.

deviation from the all months value (Fig. 7; right) compared to the first year (Fig. 7; left). This can be explained by the higher geomagnetic activity that occurred during 2000 with respect to the previous year.

MT transfer functions were obtained using the same bounded influence algorithm over the months of March and July 2000, along with jackknife estimates of the 95% confidence intervals. The apparent resistivity and phase curves display increasing error bars at longer periods (Fig. 8), reflecting a smaller number of data segments. Estimation of the transfer functions over 8 months of data (from December 1999 to August 2000 in Fig. 8) decreases the errors and stabilizes the responses at long periods. However, the observed differences between seasonal and longer term responses are not statistically significant. In general, more MT response variability was observed during the summer months.

We have observed that the magnetic transfer functions are more strongly affected by source field variability than the MT responses, as evidenced by the divergence of the induction arrows in Fig. 7. Source field effects in the MT response are second order, as suggested by Fig. 8. In addition, the seasonal variation of the electric field power spectrum is weaker than in that of the magnetic field power spectrum. A local minimum in both the north and east electric components appears in the same place (around Big and Providence Lakes; Fig. 1) regardless of the season and year. In contrast, power spectra of the horizontal magnetic field components vary from site to site distinctly between seasons, showing no common pattern for minima or maxima.

A key question is whether the source at a given time and for a selected period can be considered quasi-homogeneous over the Slave survey area (dimension $\sim 600\,\text{km} \times 600\,\text{km}$). If we can prove that non-uniform sources average out to an effective large-wavelength source over the dimensions of the array, then we can be confident that both the induction arrows and MT responses will be unbiased by source field effects.

5. Principal component (PC) analysis

For investigation of the spatial variation of the external source, we performed a principal component (or empirical orthogonal function EOF) analysis on the power spectral density matrix **S** of the magnetic field components over multiple sites. The PC analysis is

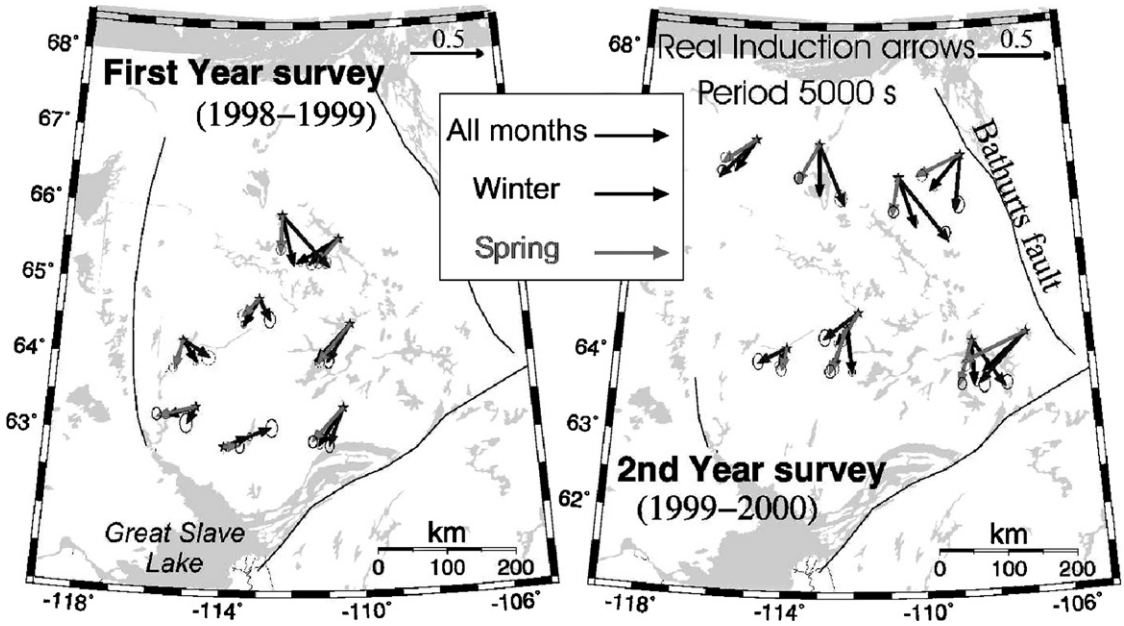

Fig. 7. Real part of the induction arrow at a period of 5000 s. Light gray and darker gray arrows were estimated from the time series over spring- and winter-time, respectively. Black arrows correspond to estimations from 8–9 months of recording (October–November to August). Ellipsoids are arrow error bounds from linear propagation of transfer functions at 95% confidence. (Left) Sites from first survey performed between October 1998 and August 1999; (right) sites from second survey performed between October 1999 and August 2000. Year 2000 was high in geomagnetic activity.

obtained from the singular value decomposition (SVD) of the matrix **S**:

$$\mathbf{S} = \mathbf{U}\Sigma\mathbf{V}^H \tag{1}$$

S is obtained from a multivariate multitaper spectral analysis (Thomson, 1982), i.e., a multivariate matrix produced by averaging multiple windowed FFTs generated with a set of orthogonal data tapering windows. It has dimension $N \times P$, where N is the number of orthogonal data tapers and P is the number of magnetic field components (time series). N is a free parameter, although increasing its value implicitly decreases the frequency resolution of the estimate.

Transforming the SVD to:

$$\mathbf{S} = \mathbf{Z}\mathbf{V}^H \tag{2}$$

yields the $N \times P$ matrix of complex principal components:

$$\mathbf{Z} = \mathbf{U}\Sigma \tag{3}$$

Z has the property of being orthogonal, i.e., $\mathbf{Z}^H\mathbf{Z} = \Sigma^2$, where $\Sigma^2 = \mathrm{diag}(\lambda_i)$, is a diagonal matrix of λ_i eigenvalues from which it is possible to assess the significance of the EOFs, and H denotes the Hermitian transpose.

The EOF vectors (**Z**) are the orthogonal modes of spatial variation of the magnetic field components (e.g., Chave et al., 1997).

Presuming that the EOF vectors have a physical meaning in terms of the source polarization, a non-uniform source incident on a conductive Earth should give EOF vectors reflecting the spatial variations of the source itself, and the number of large eigenvalues λ_i should henceforth span the dimension of the source (Egbert and Booker, 1989). However, in the presence of lateral conductivity variations in the Earth, the complex EOFs may be sensitive to both the induction and the source fields, with their relative effects unknown. Therefore, in the next sub-section we will evaluate the sensitivity of the eigenvectors to Earth's conductivity, by computing EOFs from synthetic 3D model responses that are subject to a uniform 2D polarized source.

5.1. Application to 3D model responses

Lateral conductivity variations in the crust and mantle have been demonstrated in the Slave from diverse MT surveys performed since 1996 (Jones et al., 2003). In an attempt to reconcile the 2D models obtained by the inversion of MT profile data (Jones et al., 2003) with the lake bottom data, a forward 3D model was constructed independently from the fit of the long period induction arrows (100–4000 s) of the lake and some land sites (Lezaeta et al., 2002; Jones et al., 2003). We use the electromagnetic responses of this 3D model to test the sensitivity of

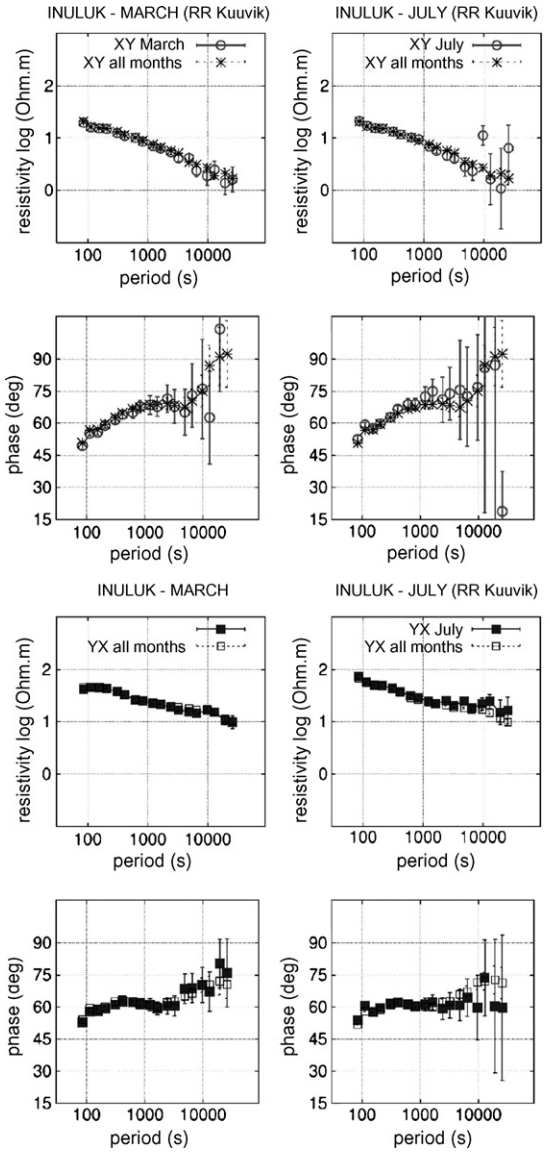

Fig. 8. Apparent resistivity (in Ω m) and phase (in degrees) for site Inuluk estimated from different seasons. Top two graphs are for the geomagnetic north polarization (*XY*) and bottom graphs for the east polarization (*YX*). Left column is for responses from March 2000 plotted over the 8 months curve (stars and open squares; from December 1999 to August 2000). Right column is for the active month of July 2000 plotted over the 8 months curve (stars and open squares).

the EOF vectors to the 3D conductivity structures of the Slave crust and upper mantle.

The modeling code used is an improved version of the Mackie et al. (1994) algorithm modified by Mackie and Booker (1999). The dimensions of the core grid are 65 × 65 nodes horizontally and 20 vertically, covering an area of 1000 km × 1000 km and 700 km depth. The source considered in this model is two horizontal/orthogonal polarizations of a uniform incident magnetic field oriented eastward (*X*) and southward (*Y*), respectively.

The horizontal magnetic field responses of $Ns = 129$ sites were used to build the frequency domain matrix **S** (Eq. (1)), obtained from the product of the $2Ns \times 2$ matrix **B** containing the two components of the horizontal magnetic fields split in two field polarizations (i.e., B_x^1, B_x^2 and B_y^1, B_y^2). This yields a square matrix for $\mathbf{S} = \mathbf{B} \cdot \mathbf{B}'$ of dimension $2Ns \times 2Ns$ and two dominant eigenvalues from Σ^2 (Eq. (3)) corresponding to the two polarization modes of the source. If the vertical component of the magnetic fields is included as additional *Ns* rows in **B**, this would yield **S** with dimension $3NS \times 3Ns$, while Σ^2 remains of rank two as the source dimension is the same. We are not including the vertical component in this analysis as its corresponding eigenvector was seen sensitive only to lateral conductivity variations when the source is a plane wave.

The complex EOF eigenvectors (**Z** in Eq. (3)) for two polarizations of a plane wave incident on a 1D Earth should yield the orthogonal modes of the spatial source variations. This means that an eastward polarization should yield a N–S eigenvector, and a southward polarization an E–W eigenvector. In the presence of lateral conductivity variations not aligned with the polarizations of the source, the EOF vectors are rotated by induction (Fig. 9 for period 120 s). However, this rotation is largely spatially uniform, and the vectors change locally in orientation and length only above zones of sharp conductivity contrasts. In the model, an example is seen at the elongated conductor at upper to mid-crustal depths following the Bathurst fault (in Fig. 7) in the eastern margin of the Slave (Fig. 9). A mantle conductor inserted in a resistive host in the model, striking NE-SW below 80 km depth in the central Slave, does not affect the eigenvectors locally as the crustal conductor in the east does, but rather affects the regional rotation of the vectors in proportion to the depth of the body. The addition of 10% random Gaussian noise to the magnetic fields (simulating normally distributed data sample) skews the orientation of the EOF vectors slightly (Fig. 10).

There are two principal eigenvectors corresponding to the dual polarizations of the source, hence the matrix of eigenvalues λ is of rank 2. The corresponding two eigenvalues should be equal in a 1D model Earth, reaching unity after normalization. For the model presented here, the two normalized eigenvalues differ at periods below 5000 s (Fig. 11). The difference between the principal eigenvalues is due to lateral conductivity variations at the corresponding penetration depths, increasing as the strength of the conductivity contrast rises. These asser-

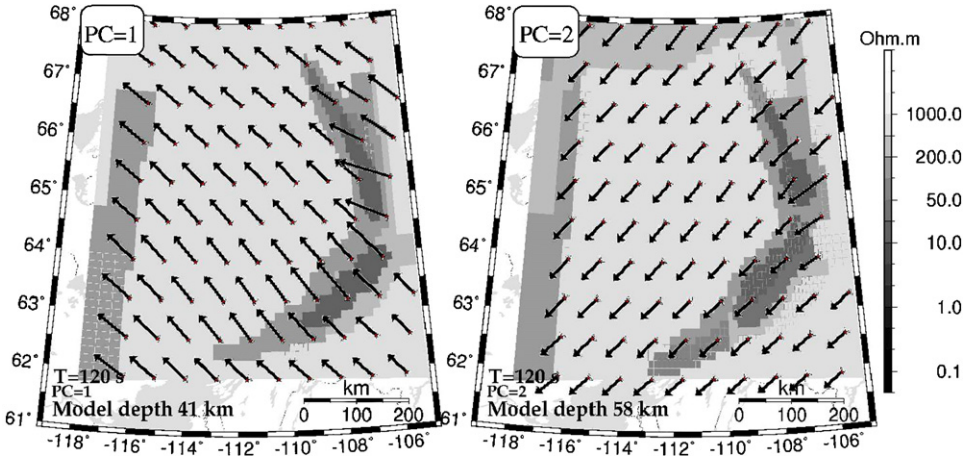

Fig. 9. Eigenvectors of the horizontal magnetic field components at a period of 120 s (see text for explanation) from the responses of a Slave 3D model with a uniform external source having two orthogonal polarizations. Superimposed in grayscale are the model resistivities (in Ω m) at a depth of 40 km (left) and 60 km (right). Dark grays represent conductive zones: (left) eigenvectors for the largest; (right) for the second largest eigenvalue.

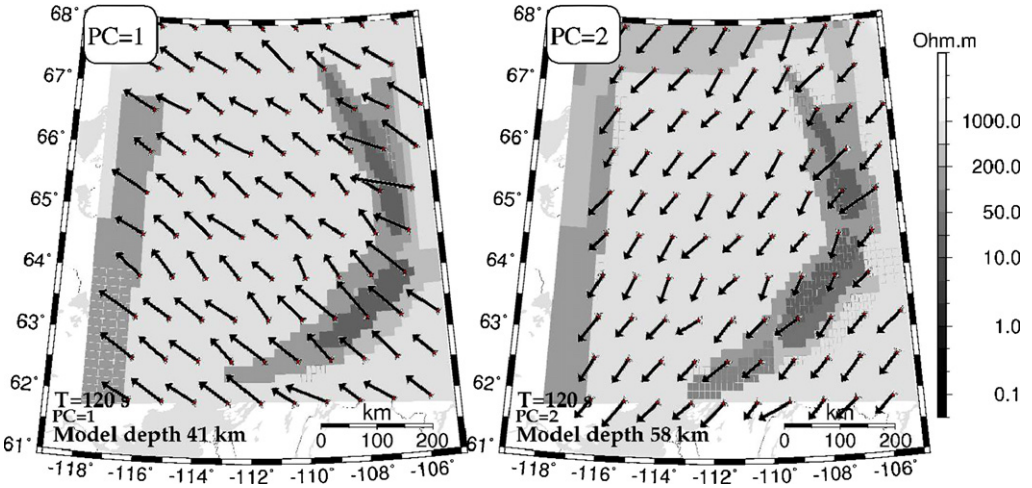

Fig. 10. Eigenvectors as in Fig. 9 after adding 10% random Gaussian noise to the magnetic field components.

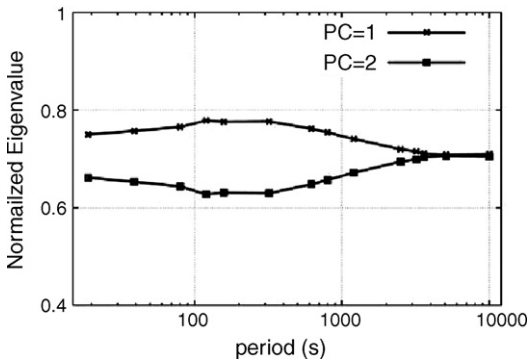

Fig. 11. Curves labeled PC = 1 and PC = 2 represent the largest eigenvalues of the principal components shown in Fig. 9, related to the two source polarizations.

tions have been tested over a range of models (not shown here).

From the 3D models tested here with the Mackie and Booker (1999) code and from other 3D thin sheet models computed with the code of Weidelt (1975), the imaginary parts of the eigenvectors are usually about 10 times smaller than the real parts. This is because the incident source is considered a uniform (unity) magnetic field, yielding a null complex phase for the eigenvectors over a 1D Earth. Any non-zero imaginary part is due to induction by lateral conductivity variations, which is typically a weak effect.

5.2. Application to field data

From the sites array, we computed frequency domain principal components from the power spectral matrix **S**

(of dimension $N \times P$) of the simultaneously recorded magnetic fields. The times series were first prewhitened over segments of several months length using a robust autoregressive filter (Chave and Thomson, 2004) to achieve better performance. Power spectra were then obtained from selected (prewhitened) time segments over P real time series using a multitaper expansion of N windows and the principal components were estimated as in Chave et al. (1997). The number of orthogonal tapers (windows) was set to $N = 32$, which turned out effective for the number of sample data considered (95,000 for a monthly time segment at sample rate 28 s). The number of columns of the matrix $\mathbf{S}$ is $P = 2Ns$, i.e., the number of time series of the two horizontal b-field components from Ns sites (8 and 9 in the first and second year surveys, respectively).

The coordinate frame of the eigenvectors is the geomagnetic north-east (25° cw from geographic north-east for the Slave). Since this coordinate frame is set a priori, any regional rotation of the eigenvectors produced by electromagnetic induction (as shown by the 3D model responses) is not evidenced in this reference frame (i.e., the coordinate of a primary two polarization spatial source dimension); however, any local deviations from this coordinate should be visible. The real and imaginary eigenvectors of the sites-array are computed from the two orthogonal PCs (north and east), which are complex numbers except for the north component of an arbitrarily chosen reference site that is real. This real north component represents a PC in-phase with the source field, whereas the out-of-phase part of the PCs is with respect to that real component. For each year-array, we chose a site located in the northern Slave for the reference (sites Inuluk; Fig. 1 and Rockh; Fig. 2), whose data is of good quality and the corresponding transfer functions show little local (near surface) conductivity effects.

For a particular eigenvalue at a given period, the two horizontal complex PCs at each site are expressed in PC phases (ϕ_x, ϕ_y) and PC amplitude (A_x, A_y), with X, Y following the geomagnetic north and east coordinates, respectively. The length of the (real or imaginary) eigenvector at each site is the magnitude of the corresponding two horizontal real (or imaginary) principal components $A_x \cos\phi_x$, $A_y \cos\phi_y$ (or $A_x \sin\phi_x$, $A_y \sin\phi_y$ if it's imaginary part). The real (or imaginary) eigenvector points according to the direction given by the arctan of the ratio between the two real (or imaginary) principal components, in analogy to the way the induction arrows are obtained.

We show the principal component analysis from the first and second years of the survey for the quiet month of March and for the active months of June–July at periods near 3000 s corresponding to eigenvector coherence above the 95% confidence limit. The first year had suitable 8 sites recorded simultaneously and the second year had 9. In the months of December–March, the first dominant eigenvector at periods over 1000 s tends to a northward orientation (Fig. 12 for 3000 s), and a similar orientation is observed in the summer of 1999 (Fig. 13; left). This reflects geomagnetic N–S variations of an E–W polarized dominant source during the summer and wintertime. The source in winter and in summer 2000 is also subject to the N–S geomagnetic variation of an E–W polarized source in the first principal eigenvalue (i.e., eigenvectors oriented NS; Fig. 13; right). We show here monthly segments to focus on an

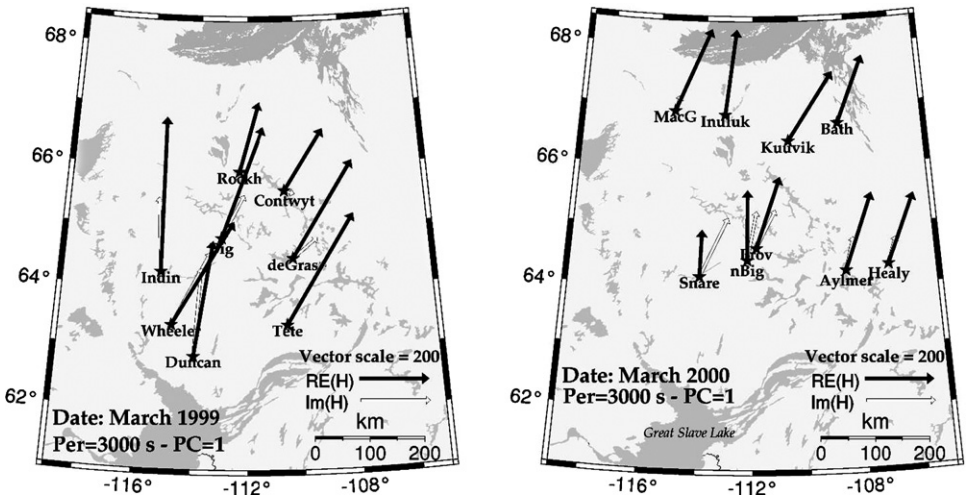

Fig. 12. Principal components (or complex eigenvectors; Re(H), Im(H)) of the largest horizontal magnetic field eigenvalue recorded during March 1999 (left) and March 2000 (right) at a period of 3000 s.

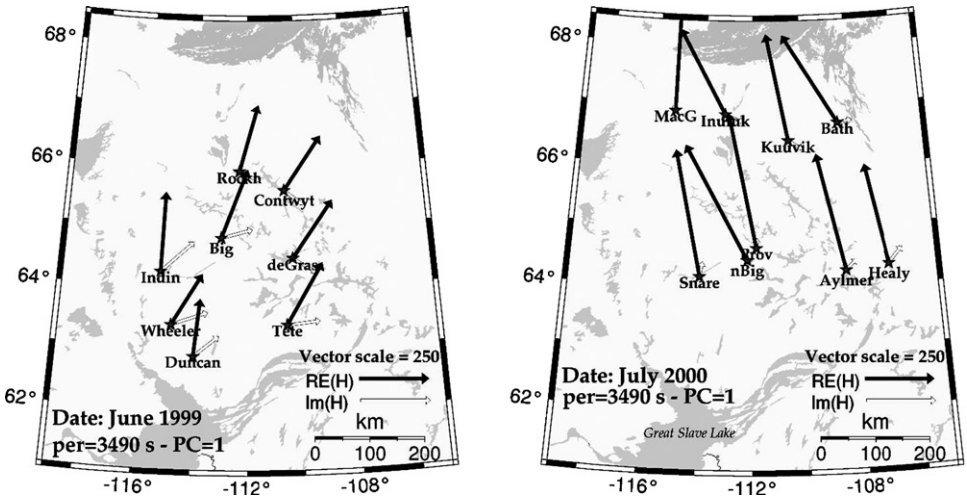

Fig. 13. Principal component of the largest horizontal magnetic field eigenvalue recorded during June 1999 (left) and July 2000 (right) at a period of 3500 s.

average representation of eigenvector directions over the month instead of weekly or short events. If there were a dominant small scale incident source over the array, this would be reflected in the eigenvector directions pointing differently among the array.

The normalized eigenvalues as a function of period vary slightly by month. A single eigenvalue dominates at periods over 10,000 s during most of the months recorded (Fig. 14), with a higher second dominant eigenvalue in the summer of 2000 (Fig. 14; right) and winter of the same year (not shown here). A dominant single eigenvalue at long periods suggests that a quasi-uniformly polarized source prevails in the corresponding energy spectrum, perhaps giving evidence of a polar electrojet since the array is in the auroral zone. Such a 1D source is considered quasi-homogeneous because the eigenvectors are relatively consistent in direction among sites (Figs. 12 and 13), thus indicating negligible source spatial variations over the array for the penetration depths under consideration.

When there are two polarizations dominating, the principal components of the second largest eigenvalue

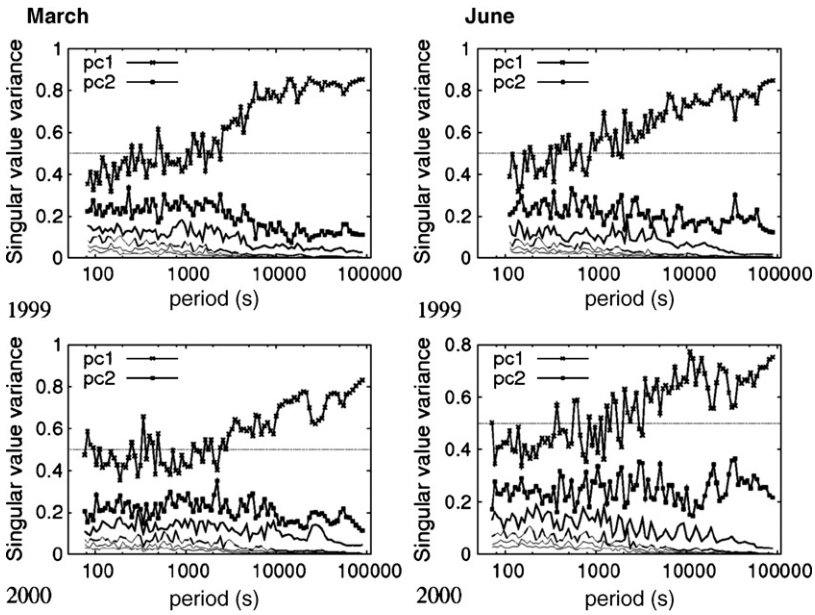

Fig. 14. First six eigenvalues as a function of period obtained from the horizontal magnetic fields recorded during March 1999 (top left), March 2000 (bottom left), June 1999 (top right) and June 2000 (top right).

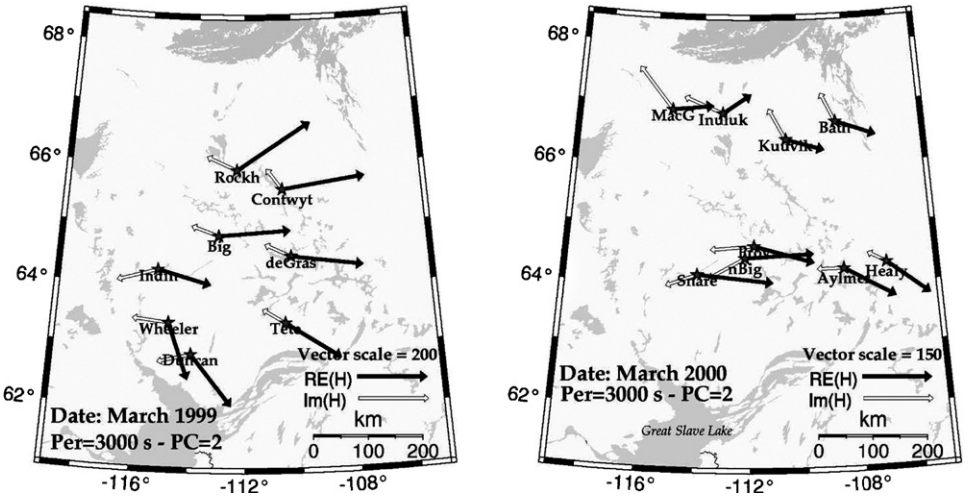

Fig. 15. Principal components as shown in Fig. 12 but corresponding to the second largest eigenvalue: (left) March 1999; (right) March 2000.

seem to be overlapped by other non-homogeneous sources because of their different eigenvector directions within the array. Fig. 15 shows the eigenvectors of the second second largest eigenvalue for March at 3000 s. These tend to point to east irregularly, but are nearly perpendicular to the corresponding first dominant eigenvectors (Fig. 12). In general, the second largest eigenvalue in the period range 4000–6000 s have high coherences (for fitting a model of SVD on the power spectra matrix) and their corresponding eigenvectors point nearly uniform within the array, although this period range sometimes varies with time. For example, in February 2000 the two dominant eigenvectors indicate a good 2D homogeneous source space (with very high coherences) at periods between 3000 and 35,000 s, while for June and July 2000 this is true in the period range 6000–35,000 and 8000–50,000 s, respectively. For March and June of 1999, the second dominant eigenvectors are fairly uniform in the period range 4000–12,000 and 4000–6000 s, respectively, displaying non-homogeneity at longer periods yet their corresponding coherences are high (March: 15,000–35,000 s; June: 7000–15,000 s). The latter indicates the effect of non-homogeneous sources during March and June 1999 at the corresponding penetration depths.

The principal components at shorter periods (100–900 s) are more difficult to interpret. These vary substantially within the array for any given month. The coherence of the eigenvectors are typically low, implying poor estimation of the principal components. This may be due to short scale ionospheric current events as well as the effect of near surface lateral conductivity contrast as demonstrated from the 3D model example.

A single dominant eigenvalue prevails at the longest periods (about a half day; 30,000–50,000 s). The corresponding eigenvectors are nearly N–S oriented at any season, hence an E–W polarized source is dominant, consistent with either an equatorial ring current source or the high latitude solar daily variation. Further, the long period principal eigenvectors are in general more uniform within the array than at periods of 1000–10,000 s, suggesting non-homogeneous spatial effects within the array at the latter period range.

6. Summary and discussion

MT/GDS responses estimated over different seasons show differences at periods over 4000 s, suggesting source field effects. However, responses obtained from over eight months of recording seem to average out the source effect variability. It is impossible to be certain that this represents a true source-free value in the absence of information about the relative bias in different seasons.

PC analysis yields the conclusion that the external source is relatively homogeneous in space (i.e, has an effective large wavelength) compared to the size of the array ($\sim 600\,\text{km} \times 600\,\text{km}$) for the longer periods under consideration (> 1000 s). At short periods, the analysis shows significant inhomogeneous spatial variations, probably due to crustal scale conductivity contrasts and irregular sources from short scale ionospheric currents within the array.

PC analysis with synthetic responses from 3D models is useful because it provides insight for the first time into the behavior of the eigenvectors and eigenvalues of uniform magnetic fields incident on a 3D conductivity Earth.

It shows that the eigenvectors of the horizontal magnetic field components are regionally rotated under the influence of regional conductivity structures. The length and direction of the eigenvectors change locally above sharp conductivity contrasts. Further, the two principal eigenvalues related to a two polarization source differ in magnitude as the conductivity contrast rises. The imaginary parts of the vectors were seen to be negligible under a uniform source.

The year 2000 was high in geomagnetic activity, and the monthly dominant principal eigenvectors from the Slave data indicate a more 2D quasi-homogeneous source space within the array for that year than during the previous year (1999). In both years, the vector orientations from the first dominant eigenvalue are fairly uniform within the array and oriented nearly N–S at periods over 1000 s, reflecting a dominant E–W polarized source of limited spatial source field inhomogeneity over the array.

Power spectra of the magnetic fields estimated over month- and day-long intervals have maxima during summertime at periods over 1000 s. In contrast, the maximum power at short periods in 2000 were seen in wintertime. At long periods, the geomagnetic north component was dominant by one or two orders of magnitude with respect to the east component, as is generally expected in high latitudes. Short period power spectra have in contrast east components that are as significant large as the north ones. This may reflect the 2D nature of ionospheric (equivalent) currents related to geomagnetic pulsations and other rapid variations, where no preferred direction of the horizontal current flow prevails. In contrast, a main 1D electrojet source may prevail at longer periods (Viljanen et al., 2001).

The nature of the source is thus different at 100–1000 s than at > 1000 s period. It seems that the source also changes in morphology among seasons at periods below a half day, suggesting a dynamic source over seasons. At long periods (> 1000 s), the year 2000 had a particular geomagnetic activity showing low energy in March and a stormy event in July. This is not typical because spring (and autumn) close to the equinox are usually more active than near the solstice (Russell and McPherron, 1973).

At a half day period (35,000–50,000 s), a single polarization source prevails at almost all seasons, manifest in a single dominant eigenvalue for the months in consideration. In the active month of July 2000 the source is 2D polarised in this period range.

In spite of a regular orientation of the principal components during the active summertime, which hints at a homogeneous spatial source, MT responses estimated in summer were worse in quality at those periods (> 1000 s) than in any other season. A PC analysis including the electric fields may help to further evaluate the source effect. However, e-fields are typically affected by direct-currents from near surface conductivity contrasts, and we suspect that their principal eigenvectors would exhibit this, obscuring the information on spatial source variation. Further, e-field power spectra of the Slave data show much less seasonal variation than the b-field power spectra. This was a reason to pay more attention to the b-fields.

Acknowledgements

We thank Jessica Spratt, Helmut Moeller, Jonathan Ware and John Bailey for their assistance in field work. We acknowledge the Space Physics Interactive Data Resource (SPIDR at http://spidr.ngdc.noaa.gov) for availability of the global geomagnetic indices. We are grateful also to the Canadian Space Agency for supplying geomagnetic data from Yellowknife. Thanks also to A. Viljanen and an anonymous reviewer for helpful suggestions and for providing information/references on source field studies. This work was supported by NSF grant EAR-9725556 and EAR-0087699 and by Fundacion Andes postdoctoral Award to P.L.

References

Chave, A.D., Luther, D.S., Filloux, J.H., 1997. Observations of the boundary current system at 26.5N in the subtropical north Atlantic ocean. J. Phys. Oceanogr. 27, 1827–1848.

Chave, A.D., Thomson, D.J., 2004. Bounded influence estimation of magnetotelluric response functions. Geophys. J. Int. 157, 988–1006.

Dmitriev, V.I., Berdichevsky, M.N., 1979. The fundamental model of magnetotelluric sounding. Proc. IEEE 67, 1034–1044.

Egbert, G.D., Booker, J.R., 1989. Multivariate analysis of geomagnetic array data. 1. The response space. J. Geophys. Res. 94, 14227–14247.

Egbert, G.D., 1989. Multivariate analysis of geomagnetic array data. 2. Random source models. J. Geophys. Res. 94, 14249–14265.

Engels, M., 1997. Untersuchungen zur elektromagnetischen Induktion in Grönland. PhD thesis. Georg-August Universität zu Göttingen, Cuvillier Verlag Göttingen, 115 pp.

Engels, M., Pulkinen, A., Viljanen, A., BEAR Working Group, 2002. Source effect modelling using the Fennoscandian 3D Earth model and equivalent current system derived from BEAR data. In: 16th Workshop on Electromagnetic Induction in the Earth, Santa Fe, New Mexico, EM4-2.

Garcia, X., Chave, A.D., Jones, A.G., 1997. Robust processing of magnetotelluric data from the auroral zone. J. Geomagn. Geoelectr. 49, 1451–1468.

Jones, A.G., Spratt, J., 2002. A simple method for deriving the uniform field MT responses in auroral zones. Earth Planets Space 54, 443–450.

Jones, A.G., Lezaeta, P., Ferguson, I.J., Chave, A.D., Evans, R.L., Garcia, X., Spratt, J., 2003. The electrical structure of the Slave craton. Lithos 71, 505–527.

Lezaeta, P., Chave, A.D., Evans, R.L., Jones, A.G., 2002. Three-dimensional electrical conductivity structure beneath the Slave Craton, NW Canada. In: SNORCLE transect Group Workshop, Sidney, BC, Canada.

Mackie, R.L., Smith, J.T., Madden, T.R., 1994. Three-dimensional electromagnetic modeling using finite difference equations: the magnetotelluric example. Radio Sci. 29, 923–936.

Mackie, R.L., Booker, J., 1999. Documentation for mtd3fwd and d3-to-mt. Unpublished user documentation. GSY-USA Inc., 2261 Market St., Suite 643, San Francisco, CA 94114.

Mareschal, M., 1986. Modelling of natural source of magnetospheric origin in the interpretation of regional induction studies: a review. Surv. Geophys. 8, 261–300.

Russell, C.T., McPherron, R.L., 1973. Semiannual variation of geomagnetic activity. J. Geophys. Res. 78, 92–108.

Schmucker, U., 1973. Regional induction studies: a review of methods and results. Phys. Earth Planet. Syst. 7, 365–378.

Thomson, D.J., 1982. Spectrum estimation and harmonic analysis. Proc. IEEE 70, 1055–1096.

Viljanen, A., Pirjola, R., Häkkinen, L., 1993. An attempt to reduce induction source effects at high latitudes. J. Geomagn. Geoelectr. 45, 817–831.

Viljanen, A., Nevanlinna, H., Pajunpaa, K., Pulkkinen, A., 2001. Time derivative of the horizontal geomagnetic field as an activity indicator. Ann. Geoephys. 19, 1107–1118.

Vozoff, P., 1972. The Magnetotelluric method in the exploration of sedimentary basins. Geophysics 37, 98–141.

Weidelt, P., 1975. Electromagnetic induction in three-dimesnional structures. J. Geophys. 41, 85–109.